Important Notice to Authors

No further publication processing will occur until we receive your response to this proof.

Attached is a PDF proof of your forthcoming article in Physical Review Fluids. Your article has 8 pages and the Accession Code is **LH16869FR**.

Please note that as part of the production process, APS converts all articles, regardless of their original source, into standardized XML that in turn is used to create the PDF and online versions of the article as well as to populate third-party systems such as Portico, Crossref, and Web of Science. We share our authors' high expectations for the fidelity of the conversion into XML and for the accuracy and appearance of the final, formatted PDF. This process works exceptionally well for the vast majority of articles; however, please check carefully all key elements of your PDF proof, particularly any equations or tables.

Figures submitted electronically as separate files containing color appear in color in the journal.

Specific Questions and Comments to Address for This Paper

1 PR Fluids prefers not to make claims of novelty or priority. Please check edits.
2 "t" roman or italic? Please check throughout.
3 References were cited out of order. Please check renumbering carefully.
4 "local gradients" meant here? Please check.
5 Π or π meant here? Please check.
6 Please check definitions for accuracy.
7 Ref. 29 was not cited in text. Please check citation here and fix if needed.
8 Please check change in figure labels from (i) (ii) etc. to (a) (b) etc. throughout.
9 Please supply article titles for all references.
Q: This reference could not be uniquely identified due to incomplete information or improper format. Please check all information and amend if applicable.

ORCIDs: Please follow any ORCID links (iD) after the author names and verify that they point to the appropriate record for each author.

Open Funder Registry: Information about an article's funding sources is now submitted to Crossref to help you comply with current or future funding agency mandates. Crossref's Open Funder Registry (https://www.crossref.org/services/funder-registry/) is the definitive registry of funding agencies. Please ensure that your acknowledgments include all sources of funding for your article following any requirements of your funding sources. Where possible, please include grant and award ids. Please carefully check the following funder information we have already extracted from your article and ensure its accuracy and completeness:

Other Items to Check

- Please note that the original manuscript has been converted to XML prior to the creation of the PDF proof, as described above. Please carefully check all key elements of the paper, particularly the equations and tabular data.
- Title: Please check; be mindful that the title may have been changed during the peer-review process.
- Author list: Please make sure all authors are presented, in the appropriate order, and that all names are spelled correctly.
- Please make sure you have inserted a byline footnote containing the email address for the corresponding author, if desired. Please note that this is not inserted automatically by this journal.

- Affiliations: Please check to be sure the institution names are spelled correctly and attributed to the appropriate author(s).
- Receipt date: Please confirm accuracy.
- Acknowledgments: Please be sure to appropriately acknowledge all funding sources.
- Hyphenation: Please note hyphens may have been inserted in word pairs that function as adjectives when they occur before a noun, as in “x-ray diffraction,” “4-mm-long gas cell,” and “*R*-matrix theory.” However, hyphens are deleted from word pairs when they are not used as adjectives before nouns, as in “emission by x rays,” “was 4 mm in length,” and “the *R* matrix is tested.”

  Note also that Physical Review follows U.S. English guidelines in that hyphens are not used after prefixes or before suffixes: superresolution, quasiequilibrium, nanoprecipitates, resonancelike, clockwise.
- Please check that your figures are accurate and sized properly. Make sure all labeling is sufficiently legible. Figure quality in this proof is representative of the quality to be used in the online journal. To achieve manageable file size for online delivery, some compression and downsampling of figures may have occurred. Fine details may have become somewhat fuzzy, especially in color figures. Figures to be published in color online will appear in color on these proofs if viewed on a color monitor or printed on a color printer.
- Please check to ensure that reference titles are given as appropriate.
- Overall, please proofread the entire *formatted* article very carefully. The redlined PDF should be used as a guide to see changes that were made during copyediting. However, note that some changes to math and/or layout may not be indicated.

Ways to Respond

- ***Web:*** If you accessed this proof online, follow the instructions on the web page to submit corrections.
- ***Email:*** Send corrections to prfproofs@aptaracorp.com
  Subject: **LH16869FR** proof corrections
- ***Fax:*** Return this proof with corrections to +1.703.791.1217. Write **Attention:** PRF Project Manager and the Article ID, **LH16869FR**, on the proof copy unless it is already printed on your proof printout.

PHYSICAL REVIEW FLUIDS **00**, 001900(R) (2020)

Rapid Communications

Liquid bridge length scale based nondimensional groups for mapping transitions between regimes in capillary break-up experiments

Karel Verbeke,[1,*] Susanna Formenti,[1,2,*] Francesco Briatico Vangosa ,[2] Christos Mitrias,[3] Naveen Krishna Reddy,[4,5] Patrick D. Anderson ,[3] and Christian Clasen [1]

[1]*Department of Chemical Engineering, KU Leuven, Celestijnenlaan 200f, 3001 Heverlee, Belgium*

[2]*Department CMIC "Giulio Natta", Politecnico di Milano, Piazza L. da Vinci 32, 20133 Milano, Italy*

[3]*Department of Mechanical Engineering, Eindhoven University of Technology, P.O. Box 513, 5600 MB Eindhoven, The Netherlands*

[4]*Hasselt University, Martelarenlaan 42, 3500 Hasselt, Belgium*

[5]*IMO-IMOMEC, Wetenschapspark 1, 3590 Diepenbeek, Belgium*

(Received 15 August 2019; accepted 1 April 2020; published xxxxxx)

Criteria to identify transitions between dynamic self-similar linear thinning regimes of liquid bridges are of utmost importance in order to accurately interpret results in capillary break-up rheometry. Currently available criteria encompass many experimental difficulties or rely on numerical approaches. Here, we introduce a different set of nondimensional groups, $\mathrm{Oh_L} = \eta_{\mathrm{in}}/\sqrt{\gamma \rho L}$ and $a = R/L$, based on the experimentally relevant axial length scale of a liquid bridge L, for viscous-dominated fluids undergoing capillary break-up in air. This framework is further extended to encompass the effect of outer viscous fluids. As a result, we present a two-dimensional operating map in which the boundaries are set by fluid properties and a single geometrical parameter, related to the experimental
1 configuration. This approach establishes guidelines to correctly interpret experimental data and identify transitions in capillary break-up experiments of liquid bridges surrounded by fluids of different viscosities.

DOI: 10.1103/PhysRevFluids.00.001900

Capillary break-up has been extensively employed in the past as a tool to study the thinning behavior of complex fluid bridges and to extract material properties in extensional flows such as the transient (apparent) extensional viscosity, or the longest relaxation time [1,2]. Nonetheless, a successful application of this technique relies on a proper identification of the underlying dynamics, originating either from a balance or dominance of single material properties that causes the
2 minimum liquid bridge radius R_{min} to exhibit a certain scaling $R_{\mathrm{min}} = Hf(\mathrm{t})$, with $f(\mathrm{t})$ some function of time t. In most cases, similarity solutions were needed to determine the necessary numerical prefactors H for a quantitative evaluation of a scaling regime [3]. A multitude of dynamical regimes and $f(\mathrm{t})$, such as viscocapillary (V) [4], elastocapillary (EC) [5], inertia capillary (IC) [6,7], and inertia viscous (IV) [8], have been identified in the literature based on the relevant force balance. Additional regimes were highlighted in more complex scenarios, for instance, when the viscosity of the surrounding fluid cannot be neglected [two-fluid viscous (LV) and line-sink flow
3 (LSF) regimes [9,10]], for bubbles undergoing capillary thinning in fluids of various viscosities [11] or for confined flows [12]. A comprehensive description can be found in Refs. [1,13,14].

Intensive theoretical studies, usually based on scaling arguments, were carried out to formulate criteria that allow one to identify the presence of these regimes and their transitions [13,15]. This

*These authors contributed equally to this work.

is in particular necessary for regimes that exhibit the same $f(\mathrm{t})$ [as the linear V, IV, and LV (LSF) regimes], so that an experimentally observed scaling is not sufficient for their identification. However, Eggers and Villermaux [13] address that discrepancies exist between proposed criteria for V to IV transitions and experimental observations [16,17], possibly depending on the overall geometry, which can also be seen in Ref. [18]. One cause lies in limitations to access criteria that focus on the thinning stages close to break-up, hence close to or below (optical) resolution
4 limits. Second, effective criteria based on local velocities, local gradients, or Reynolds numbers [19] require information that is hardly experimentally available and rely on numerical calculations. Third, and most important, the experimental axial length scales of the liquid bridge have so far not been taken into account. Although case-specific geometrical parameters were employed to determine global behavior and regime transitions, they are usually buried in prefactors and arbitrary constants.

The purpose of this Rapid Communication is therefore to establish a systematic framework to identify transition criteria between linear thinning regimes in liquid bridges, solely based on material properties and characteristic dimensions of different experimental setups. To this end, we introduce a set of nondimensional groups based on the experimentally relevant axial length scale of the liquid bridge. The concept of an axial Ohnesorge number $\mathrm{Oh_L}$, along with the nondimensional radius a, is initially introduced for Newtonian, viscous-dominated fluids undergoing capillary break-up in air. Subsequently, the analysis is extended to encompass the effect of outer fluids of significant viscosity. Experimental limits, which depend on the setup configuration, are employed to identify the observable regimes and their transitions. As a result, a two-dimensional (2D) operating map, in which the boundaries are set by our dimensionless groups and the dependent scaling relations, is introduced. This map is an alternative guideline to identify regimes and interpret experimental observations for viscous liquids surrounded by air and fluids of different viscosities.

For Newtonian fluids, the balance controlling the radial thinning behavior has been given in terms of the global Ohnesorge number $\mathrm{Oh} = \eta_{\mathrm{in}}/\sqrt{\gamma\rho R}$ that compares radial viscous and inertial contributions (where η_{in} is the shear viscosity, γ the surface tension, ρ the density, and R the characteristic radial dimension of the liquid bridge). For a viscous-dominated thinning (V regime), Papageorgiou [4] exploited a similarity solution to show that the prefactor in the linear decay of the minimum radius of a slender liquid bridge $R_{\mathrm{min}} \sim -H\gamma t/\eta_{\mathrm{in}}$ takes on the value $H = 0.0709$ [20]. As the liquid bridge thins, inertia becomes progressively more significant [21], leading eventually to a transition to the also linear inertia-viscous regime (IV), for which $H = 0.0304$ [8]. However, as indicated above, a transition criterion between the V and IV regime that scales with Oh [13] deviates up to orders of magnitude for different experimental setups. We propose that the underlying difference between the experiments is the length L of the liquid bridge, which is so far missing in the dimensional analysis. Including an axial length scale L, it is straightforward to show that the
5 Buckingham Π theorem yields as one possible solution for the now two alternative groups

$$\mathrm{Oh_L} = \frac{\eta_{\mathrm{in}}}{\sqrt{\gamma\rho L}}, \quad a = \frac{R}{L}, \tag{1}$$

and thus as a transition criterion, $\mathrm{Oh_L^2}a$ that can also be derived balancing axial inertial and viscous stresses. Both groups now incorporate with the axial length scale L an unconventional nondimensionalization of the fluid properties that captures, however, the essential geometrical differences between experimental setups, which was generally not possible with the traditional nondimensionalization using an often arbitrary initial radial length R. In the most commonly used
6 capillary break-up techniques, the liquid bridge is held between two fixed boundaries: in capillary break-up extensional rheometry (CaBER) experiments [20] between circular plates, with adjustable distances of O(1 cm), in a Rayleigh-Ohnesorge jetting extensional rheometer (ROJER) [22] between equidistant [O(100 μm)] droplets on a flying jet, while dripping-onto-substrate extensional rheometry (DOS) [23] probes a liquid bridge of O(1 mm) confined between a nozzle and a substrate. Contrary to unconfined liquid *filaments*, extensively studied by Schulkes, Basaran,

and Hutchings [24–27], the liquid *bridge* length (and thus L) is fixed for a capillary break-up experiment [13], but differs up to two orders of magnitude between the different configurations.

The significance of the axial length scale is supported by a transition criterion between the V and IV regime recently introduced by Li and Sprittles [28], which they suggested to take place when the local Reynolds number $\mathrm{Re} = \rho u L/\eta_{\mathrm{in}}$ (where u is the local axial velocity at an axial distance L away from the point of minimal axial velocity) reaches at the point of maximum axial velocity $u_{\max}$ (at $L_{\max}$) a critical value of $\mathrm{Re} = 0.85$. One can decouple Re (and conveniently avoid the experimentally difficult to access local velocity) into $\mathrm{Oh_L}$ and a by approximating the slender liquid bridge with a cylindrical geometry. Replacing in Re the axial velocity via the strain rate $\dot{\varepsilon} = u/L = -2\dot{R}/R$, using the linear radius decay of Papageorgiou for viscous fluids [4], yields $\mathrm{Re} = (2H\rho\gamma L^2)/(\eta_{\mathrm{in}}^2 R) = 0.1418/(\mathrm{Oh_L^2} a)$.

V to IV. We can now determine the critical transition criteria for the dimensionless radius a exclusively based on fluid properties using the axial $\mathrm{Oh_L}$ of Eq. (1), once the critical liquid bridge length scale L is introduced. Without recurring to numerical methods, a critical axial length scale L, defined as the axial distance $L_{\max}$ between the point of maximum and zero axial velocity (analogously to Ref. [28]), can be accessed from the velocity profiles derived from the experimentally obtained liquid bridge shapes. In the V regime, this $L_{\max}$ is predicted to scale with time only as $\sim(t_b - t)^{0.175}$ [3,4], and this near time independence has been numerically [28] and experimentally (see the Appendix) confirmed. Using the numerically determined transition criterion of $\mathrm{Re} = 0.85$ [28] would give $(\mathrm{Oh_L^2} a)_{\mathrm{crit}} = 0.17$. However, taking into account the experimentally observed deviations from the ideal cylindrical shape via an experimentally observed correction factor of 1.5 (see the Appendix) gives for the transition from V to IV,

$$a_{\mathrm{crit}} = \frac{R_{\mathrm{crit}}}{L} = \frac{0.11}{\mathrm{Oh_L^2}}. \tag{2}$$

V to LV. Next, we apply this alternative nondimensionalization via L to identify the transitional criteria also in the presence of an outer immiscible fluid of significant viscosity, assuming the inner
7 fluid to be incompressible and the density mismatch between the two fluids $\Delta\rho$ insignificant [29,30]. Lister and Stone [9] have shown that, even for low viscous outer fluids, the drag exerted by the outer liquid can no longer be neglected when break-up is approached. Introducing the nondimensional viscosity ratio $p = \eta_{\mathrm{in}}/\eta_{\mathrm{out}}$ of inner to outer fluid, for $p \gg 1$ the flow inside the liquid bridge is predominantly a uniaxial extension and causes a radially decaying shear drag on the outer fluid [see
8 Fig. 1(a)]. They approximated this drag as the shear stress induced by a cylinder sliding axially through the outer fluid, yielding the momentum balance [in terms of a of Eq. (1)],

$$\frac{\gamma}{R} = 3p\eta_{\mathrm{out}}\dot{\varepsilon} - \frac{B\eta_{\mathrm{out}}}{2a^2}\dot{\varepsilon}, \tag{3}$$

where $B = 2/|\ln a|$ is a dimensionless coefficient [9]. The dimensionless group that arises when balancing inner and outer fluid stresses on the right-hand side of Eq. (3) is $pa^2|\ln a|$, which describes the transition from the V regime, where viscous stresses generated by the outer fluid are negligible, to one in which they control the thinning behavior (LV). Again, we can describe the transition in terms of a critical radius,

$$a_{\mathrm{crit}}^2|\ln a_{\mathrm{crit}}| = \frac{1}{3p}. \tag{4}$$

LSF to LV. As pointed out by Sierou and Lister [10], a drastically different physical picture is seen for small viscosity ratios ($p \ll 1$). In the outer fluid, the flow is a nearly pure radial extension, resembling a line distribution of sinks, while a parabolic shear (Poiseuille) flow occurs in the inner liquid, as illustrated in Fig. 1(a). The momentum balance takes on the form

$$\frac{\gamma}{R} = \frac{4up\eta_{\mathrm{out}}L}{R^2} + \eta_{\mathrm{out}}\frac{u}{L}, \tag{5}$$

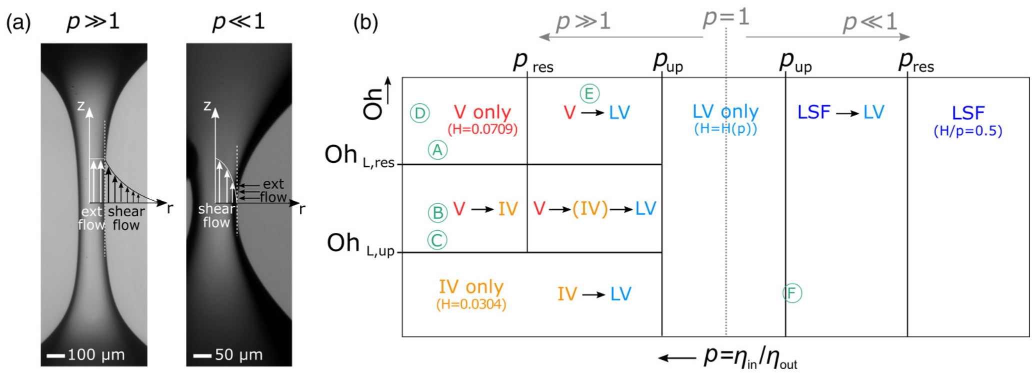

FIG. 1. (a) High-resolution images from CaBER experiments performed with a surrounding immiscible outer liquid ($p^{\gg 1} = 18.7$ and $p^{\ll 1} = 0.002$). The schematics highlights the differences in the expected inner and outer flow profiles for $p \gg 1$ and $p \ll 1$, respectively. (b) 2D operating map as a function of the dimensionless groups $\mathrm{Oh_L}$ and p. The derived criteria are used to delimit the areas within which specific regimes and transitions can be experimentally detected. Circled green letters corresponds to the capillary break-up experiments for various L, and inner and outer fluid viscosities of Fig. 2.

in which u is the radially averaged velocity in the axial direction in the inner fluid. Balancing the two terms on the right-hand side in Eq. (5) establishes the transition from a thinning regime dominated by the radial drag of the outer fluid [line-sink flow (LSF)] to the point where viscous friction of the inner fluid can no longer be neglected (LV), and determines a dimensionless group p/a^2. The critical transition criterion can then be rewritten as

$$a_{\mathrm{crit}} = \sqrt{4p}. \tag{6}$$

Observation limits for transitions. The transitional criteria for a introduced above are defined solely based on material properties and one geometrical parameter via the dimensionless groups $\mathrm{Oh_L}$ and p. It is crucial to note that an a_{crit} can vary significantly for the same fluid due to the intrinsically different axial dimensions and length scales L employed in the various capillary break-up techniques CaBER [20], DOS [23], and ROJER [22]. This also entails that the same regimes and transitions might not necessarily be observable in capillary break-up experiments performed on the same fluid, but with different techniques (and thus different L). However, since L is observed to not change significantly in time in the V regime, this geometry-dependent length scale can be used to assess the observation range for different setups. The derived transitional criteria can be reworked as

$$\mathrm{Oh_L} = \sqrt{\frac{0.11}{a_{\mathrm{crit}}}}, \qquad p^{\gg 1} = \frac{|\ln(a_{\mathrm{crit}})|^{-1}}{3a_{\mathrm{crit}}^2}, \qquad p^{\ll 1} = \frac{a_{\mathrm{crit}}^2}{4}. \tag{7}$$

Setting a_{crit} equal to the upper and lower observation limits of the radius for a given L of a setup allows us to determine *a priori* for which $\mathrm{Oh_L}$, $p^{\gg 1}$, or $p^{\ll 1}$ an a_{crit} can be experimentally observed. Since most regimes are based on a slenderness assumption (i.e., $a = R/L \ll 1$), a first limit is set by an upper radius R_{up}, so that $a_{\mathrm{crit}} \leqslant a_{\mathrm{up}} = R_{\mathrm{up}}/L$ in order for a transition to be observable. Using Eq. (7), a_{up} identifies then the critical global $\mathrm{Oh_{L,up}}$ below which no transition but only the IV regime is observed. Similarly, the upper slenderness limit a_{up} can also be used to determine the viscosity ratio $p_{\mathrm{up}}^{\gg 1}$ below which only the LV regime is visible for a set L. An upper criterion for $p \ll 1$ can, however, not be derived based on the same argument in a straightforward fashion. Due to the quadratic nature of the liquid bridge profile in the LSF regime [32], L is much smaller compared to the other cases [see, for example, the image for $p \ll 1$ in Fig. 1(a)] and the bridge only becomes sufficiently slender when the transition to LV itself takes place. Nonetheless, a slenderness-based limit $p_{up}^{\ll 1}$ can still be used to determine the critical viscosity ratio below which the LSF regime can be detected right before transitioning to the slender LV regime.

The lower critical boundary is set by the radial resolution limit R_{res}, which varies significantly with the experimental detection technique [11] and is usually disregarded in numerical studies. As for the upper limit, from $a_{crit} \geqslant a_{res} = R_{res}/L$, the lower limits $\mathrm{Oh}_{L,res}$, $p_{res}^{\gg 1}$, and $p_{res}^{\ll 1}$ are obtained from Eq. (7).

All the aforementioned limits are illustrated in Fig. 1(b) where a 2D map describes the observable regimes and transitions in terms of Oh_L and p and thus the respective radii (once the fluid properties and in particular the axial length L of the setup are known).

Experimental verification. To verify our introduced criteria and limits, we use the map in Fig. 1(b) to predict the behavior and transitions for a number of experiments encompassing the 2D parameter space. The capillary break-up experiments are performed using a CaBER rheometer (Thermo Haake, high-speed video-imaging re-equipped). a_{up} is calculated assuming a slenderness limit $L/R = 10$ [28], and a_{res} is calculated based on the limit of the optical setup, which can accurately resolve down to a radius of 5 μm. The geometrical parameter L is determined following the Appendix, and is experimentally found to be directly related to the final plate separation distance. Water and glycerol-water mixtures are used as inner fluids, and air and silicon oils of different viscosities as outer fluids.

To show the importance of the geometry to determine the onset of the V to IV transition, in a first series of experiments [A, B, and C in Fig. 1(b)] we move through the map down the vertical axis for a high, fixed value of p. The experiments are performed with the same inner fluid ($\eta_{in} = 0.365$ Pa s, $\gamma = 65$ mN m) surrounded by air ($p = 24\,333$), while the geometrical factor L is changed by varying the final plate distance. The temporal evolution of the minimum radius is shown in Fig. 2(a) for the three cases, together with the thinning predictions for the V regime ($H = 0.0709$) and the IV regime ($H = 0.0304$). Figure 2(a) clearly illustrates how the window between R_{up} and R_{crit} for the observation of a transition, drastically increases by increasing L. Moreover, R_{crit} markedly corresponds to the radius at which experimental data start deviating from the theoretical V thinning, thus accurately predicting the onset of a transition to IV. A second series of experiments [D and E in Fig. 1(b)] shows the effect of increasing viscosity of the outer fluid while keeping L and inner fluid properties constant ($\eta_{in} = 0.518$Pa s). With air as the outer fluid, case D ($p = 34\,435$) is comparable to case A, where the transition to IV is below the resolution limit, as shown by the minimum radius evolution in Fig. 2(b). By adding an outer liquid of sufficiently high viscosity ($p = 96$), R_{crit} calculated with Eq. (4) lies now within the experimentally detectable range and nicely corresponds to the experimentally observed onset of the LV regime in Fig. 2(ii). Moving to the other side of the map towards low viscosity ratios, case F in Fig. 1(ii) ($\eta_{in} = 10^{-3}$ Pa s, $p = 0.002$) represents an area of the map at the limits of experimental accessibility. Nonetheless, the R_{min} evolution in Fig. 2(c) shows that Eq. (6) precisely predicts the transition from LSF to LV.

To conclude, in this Rapid Communication, we introduce a theoretical framework for capillary break-up experiments to determine the critical transition radii between dynamical regimes when viscous stresses are governing the inner or outer fluid flows (or both). Our criteria depend solely on fluid properties via an alternative set of nondimensional groups incorporating the axial length scale L of the liquid bridge, which is for slender filaments in the V regime directly related to the axial dimension of the experimental setup. The criteria describe a 2D map to be used as a guideline to correctly pinpoint the observability of transitions between linear thinning regimes in experiments, as proven by examples covering a wide parameter range. Still, further experiments are needed to refine the inner part of the parameter space. In particular, the IV to LV transition is indicated to take place at $a \sim p^{-1/2}$ [9], but the correlation of the length scale L to the geometrical parameters of the bridge in the IV regime is unexplored. A full comprehension of predominantly viscous fluids will allow us to expand the map to more difficult scenarios, including the presence of viscoelasticity, for which the operating space could be expanded to 3D by introducing the Deborah (De) or Weissenberg (Wi) numbers.

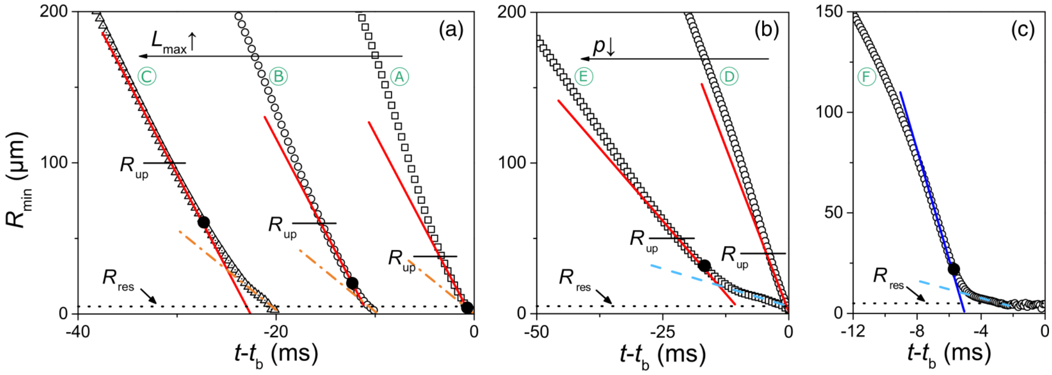

FIG. 2. Minimum radius evolution ($R_{\min}$) in time, with t_b as the break-up time, for several fluids and geometrical conditions in CaBER experiments performed in air [(a), (b) (open circles)] and with an outer liquid [(b) (open squares), (c)]. Solid dots represent calculated R_{crit}. Thinning curves in A are shifted 10 ms apart for clarity. (a) Experimentally detectable regimes are determined by the set geometrical conditions. For the same fluid ($\eta_{\text{in}} = 0.365$ Pa s, $\gamma = 65$ mN m), R_{crit} via Eq. (2) shifts to larger radii and the experimental window (R_{up}-R_{res}) expands as the geometrical parameter L increases (right to left: 480, 600, and 1000 μm). Consistently, the thinning dynamics appear to be solely V dominated for the lowest L (open squares), whereas a region following the IV scaling is clearly distinguishable for the highest L (open triangles). R_{crit} predicted with Eq. (2) matches the deviation of the data from the predicted V scaling ($H = 0.0709$, red solid line) towards the IV scaling ($H = 0.0304$, orange dashed-dotted line). (b) Thinning curves of the same inner fluid ($\eta_{\text{in}} = 0.518$ Pa s, $\gamma = 63.7$ mN m and 30.0 mN m for D and E, respectively) at comparable geometrical conditions show different behaviours depending on the outer medium viscosity. For $p \gg 1$, the transition from V ($H = 0.0709$, red solid line) to LV regime [$H(\text{p}) = 0.02$ [31], blue dashed line] is detectable only if η_{out} is sufficiently high to fulfill the condition $p_{\text{res}} \ll p \ll p_{\text{up}}$ (open circles $p = 34435$, open squares $p = 96$). (c) For $p = 0.002$, R_{crit} according to Eq. (4) correspond to the deviation from LSF ($H = 0.5$, blue solid line) to the LV regime [$H(\text{p}) = 0.04$ [10], blue dashed line].

APPENDIX

To decouple Re into Oh_{L} and a, the liquid bridge was approximated as a perfect cylinder for which the axial velocity $u = \dot{L}$ increases linearly along the bridge axis. Nonetheless, actual fluid bridges exhibit an axial curvature [Fig. 3(a)], which causes a significant deviation of $u(z)$ from linearity. Here, we introduce an experimental method to determine the radially averaged axial velocity $u_{\text{a}}(z,t)$, a numerical correction factor C accounting for this deviation for the determination of a_{crit} [Eq. (2)], and the length $L_{\max}$ at $u_{\text{a,max}}$.

$u_{\text{a}}(z,t)$ [Fig. 3(b)] can directly be obtained from the experimentally observed evolution of the bridge shape, following the approach of Rothert *et al.* [16]. For this the cumulative volume $V_{\text{cumul}}(z = z_0 + i\Delta z, t) = \sum_{z_0}^{z_0+i\Delta z} \Delta z \pi R^2(z_0 + i\Delta z, t)$ is determined from the radius evolution [with $z_0(t)$ the position of the minimum radius and Δz the pixel size]. Assuming zero axial velocity at $z_0(t)$, the axial velocity at position z is

$$u_{\text{a}}(z,t) = \frac{1}{\pi R^2(z,t)} \frac{dV_{\text{cumul}}(z,t)}{dt}. \tag{A1}$$

Due to axial curvature at the bridge end bulges, the actual average axial velocity profile exhibits a sinusoidal shape [Fig. 3(b)], allowing us to determine a $u_{\max}$ at $L_{\max}$. Plotting $L_{\max}(t)$ in Fig. 3(c) shows that, within the V regimes, $L_{\max}$ remains approximately constant for different experimental conditions of Fig. 2. The inset in Fig. 3(b) shows the overestimation of the velocity at $z = L_{\max}$ when assuming a linear increase of u with z. Evidently, also the calculated R_{crit} in Fig. 3 (solid dot, calculated from $a_{\text{crit}} = R_{\text{crit}}/L_{\max} = 0.17\,\text{Oh}_{\text{L}}^2$) lies then above the actual transition radius compared

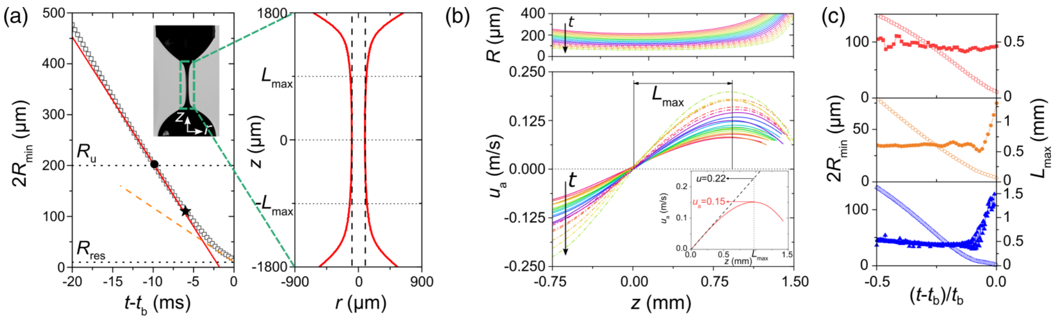

FIG. 3. (a) Capillary thinning evolution of a Newtonian fluid with $\eta_{in} = 0.365$ mPa s in air and with $L_{max} = 900\ \mu$m. R_{crit} calculated from the linear evolution of u (black solid dot, high-resolution image in the inset) overestimates the V to IV transition, which is instead correctly captured by R_{crit} calculated incorporating the corrective factor C in Eq. (2) (black solid star). The enlargement of the inset shows the visible difference between the ideal cylinder geometry (black dashed lines) and the actual profile (red solid lines). (b) Temporal evolution of $R(z)$ and $u_a(z)$ in a capillary break-up experiment of a glycerol-water mixture in air ($\eta_{in} = 0.365$ mPa s) with $L_{max} = 900\ \mu$m (-18.33 ms $< t - t_b < -6.33$ ms at $\Delta t = 0.66$ ms). Inset: The deviation of the real profile from the ideal cylinder geometry implicates the large difference at L_{max} between $u_a = 0.15$ m/s (red solid line) and $u = 0.22$ m/s (black dashed line) calculated assuming a linear evolution of the axial velocity. (c) Direct comparison between the temporal evolution of R_{min} (open symbols) and L_{max} (solid symbols), determined from the experimental u_a profiles. The characteristic length remains approximately constant throughout the complete bridge evolution for case A of Fig. 2 (top, red squares). Also for cases B (middle, orange circles) and E (bottom, blue triangles) L_{max} remains constant in the V regime, up to the transitions to the asymmetrical thinning regimes (IV or LV).

to experimental data, while the theoretical V and IV scalings (red solid and orange dashed lines, respectively) suggest a much later transition. To correct for this overestimation, $C = u_{act}/u$ at L_{max} has been calculated for several CaBER experiments performed on V-dominated fluids at different L. Remarkably, C assumes a constant value of 1.5, and is used to quantitatively correct the criterion derived for a_{crit} [Eq. (6)]. The corrected R_{crit} [Fig. 3(a), black solid star] corresponds then to the deviation from the V scaling, indicating the transition to the IV regime.

Q

[1] G. H. McKinley, Visco-elasto-capillary thinning and break-up of complex fluids, Rheol. Rev. **3**, 1 (2005).
[2] C. Clasen, P. M. Phillips, L. Palangetic, and J. Vermant, Dispensing of rheologically complex fluids: The map of misery, AIChE J. **58**, 3242 (2012).
[3] J. Eggers, Nonlinear dynamics and breakup of free-surface flows, Rev. Mod. Phys. **69**, 865 (1997).
[4] D. T. Papageorgiou, On the breakup of viscous liquid threads, Phys. Fluids **7**, 1529 (1995).
[5] V. Entov and E. Hinch, Effect of a spectrum of relaxation times on the capillary thinning of a filament of elastic liquid, J. Non-Newtonian Fluid Mech. **72**, 31 (1997).
[6] Y. Chen and P. Steen, Dynamics of inviscid capillary breakup: Collapse and pinchoff of a film fridge, J. Fluid Mech. **341**, 245 (1997).
[7] R. F. Day, E. J. Hinch, and J. R. Lister, Self-Similar Capillary Pinchoff of an Inviscid Fluid, Phys. Rev. Lett. **80**, 704 (1998).
[8] J. Eggers, Universal Pinching of SD Axisymmetric Free-Surface Flow, Phys. Rev. Lett. **71**, 3458 (1993).
[9] J. R. Lister and H. A. Stone, Capillary breakup of a viscous thread surrounded by another viscous fluid, Phys. Fluids **10**, 2758 (1998).
[10] A. Sierou and J. R. Lister, Self-similar solutions for viscous capillary pinch-off, J. Fluid Mech. **497**, 381 (2003).

[11] J. C. Burton, J. E. Rutledge, and P. Taborek, Fluid Pinch-Off Dynamics at Nanometer Length Scales, Phys. Rev. Lett. **92**, 244505 (2004).

[12] A. A. Pahlavan, H. A. Stone, G. H. McKinley, and R. Juanes, Restoring universality to the pinch-off of a bubble, Proc. Natl. Acad. Sci. USA **116**, 13780 (2019).

[13] J. Eggers and E. Villermaux, Physics of liquid jets, Rep. Prog. Phys. **71**, 1 (2008).

[14] S. L. Anna, Droplets and bubbles in microfluidic devices, Annu. Rev. Fluid Mech. **48**, 285 (2015).

[15] O. A. Basaran, Small-scale free surface flows with breakup: Drop formation and emerging applications, AIChE J. **48**, 1842 (2002).

[16] A. Rothert, R. Richter, and I. Rehberg, Formation of a drop: Viscosity dependence of three flow regimes, New J. Phys. **5**, 1 (2003).

[17] A. Rothert, R. Richter, and I. Rehberg, Transition from Symmetric to Asymmetric Scaling Function before Drop Pinch-Off, Phys. Rev. Lett. **87**, 084501 (2001).

[18] W. Mathues, C. McIlroy, O. G. Harlen, and C. Clasen, Capillary breakup of suspensions near pinch-off, Phys. Fluids **27**, 093301 (2015).

[19] J. R. Castrejón-Pita, A. A. Castrejón-Pita, S. S. Thete, K. Sambath, I. M. Hutchings, J. Hinch, J. R. Lister, and O. A. Basaran, Plethora of transitions during breakup of liquid filaments, Proc. Natl. Acad. Sci. USA **112**, 4582 (2015).

[20] G. H. McKinley and A. Tripathi, How to extract the Newtonian viscosity from capillary breakup measurements in a filament rheometer, J. Rheol. **44**, 653 (2000).

[21] M. P. Brenner, J. R. Lister, and H. A. Stone, Pinching threads, singularities and the number 0.0304, Phys. Fluids **8**, 2827 (1996).

[22] V. Sharma, S. J. Haward, J. Serdy, B. Keshavarz, A. Soderlund, P. Threlfall-Holmes, and G. H. McKinley, The rheology of aqueous solutions of ethyl hydroxy-ethyl cellulose (EHEC) and its hydrophobically modified analogue (hmEHEC): Extensional flow response in capillary break-up, jetting (ROJER) and in a cross-slot extensional rheometer, Soft Matter **11**, 3251 (2015).

[23] J. Dinic, Y. Zhang, L. N. Jimenez, and V. Sharma, Extensional relaxation times of dilute, aqueous polymer solutions, ACS Macro Lett. **4**, 804 (2015).

9 [24] A. A. Castrejón-Pita, J. R. Castrejón-Pita, and I. M. Hutchings, Phys. Rev. Lett. **108**, 074506 (2012).

[25] P. K. Notz and O. A. Basaran, J. Fluid Mech. **512**, 223 (2004).

[26] R. M. S. M. Schulkes, J. Fluid Mech. **309**, 277 (1996).

[27] C. R. Anthony, P. M. Kamat, M. T. Harris, and O. A. Basaran, Phys. Rev. Fluids **4**, 093601 (2019).

[28] Y. Li and J. E. Sprittles, Capillary breakup of a liquid bridge: Identifying regimes and transitions, J. Fluid Mech. **797**, 29 (2016).

[29] J. Eggers and T. F. Dupont, Drop formation in a one-dimensional approximation of the Navier-Stokes equation, J. Fluid Mech. **262**, 205 (1994).

[30] I. Cohen and S. R. Nagel, Testing for scaling behavior dependence on geometrical and fluid parameters in the two fluid drop snap-off problem, Phys. Fluids **13**, 3533 (2001).

[31] I. Cohen, M. P. Brenner, J. Eggers, and S. R. Nagel, Two Fluid Drop Snap-Off Problem: Experiments and Theory, Phys. Rev. Lett. **83**, 1147 (1999).

[32] P. Doshi, I. Cohen, W. W. Zhang, M. Siegel, P. Howell, O. A. Basaran, and S. R. Nagel, Persistence of memory in drop breakup: The breakdown of universality, Science **302**, 1185 (2003).